Nature Environment and Pollution Technology
An International Quarterly Scientific Journal

p-ISSN: 0972-6268
(Print copies up to 2016)
e-ISSN: 2395-3454

Vol. 23 | No. 4 | pp. 1973-1993 | 2024

Original Research Paper

https://doi.org/10.46488/NEPT.2024.v23i04.007

Open Access Journal

Landslide Susceptibility Zonation Mapping Using Machine Learning Algorithms and Statistical Prediction at Hunza Watershed Basin, Pakistan

A. Khan[1†], G. Khan[1], M. Minhas[2, 3], S. A. Hussain Gardezi[5, 6, 7], J. Ahmed[2, 4] and N. Abbas[1, 2]

[1]Department of Earth Sciences, Karakoram International University (KIU), Gilgit, 15100, Pakistan
[2]Faculty of Land Resources Engineering, Kunming University of Science and Technology, Yunnan, 650093, China
[3]Centre of Excellence in Mineralogy, University of Balochistan, Quetta, Pakistan
[4]Department of Geology, University of Balochistan, Quetta, Pakistan
[5]Key Laboratory of Ocean and Marginal Sea Geology, South China Sea Institute of Oceanology, Chinese Academy of Science, Guangzhou, 510301, China
[6]University of Chinese Academy of Science, Beijing, 100049, China
[7]Azad Jammu and Kashmir Directorate, Geological Survey of Pakistan, Muzaffarabad13100, Pakistan
†Corresponding author: Asghar Khan: Asghar.khan@kiu.edu.pk

Nat. Env. & Poll. Tech.
Website: www.neptjournal.com

Received: 14-01-2024
Revised: 04-03-2024
Accepted: 02-04-2024

Key Words:
Seed cell area index
Intuitionistic fuzzy divergence
Karakoram highway
Susceptibility mapping
Prediction rate curve

ABSTRACT

The mountainous region of the Hunza River watershed basin, especially along the Karakorum highway, and also known as a third pole for the high accumulation of glaciers, which leads to huge devastating landslides occurring every year. Landslide susceptibility mapping was carried out using two deep machine learning techniques (DeeplabV3$^+$ & universal network U-Net) and two statistical models (Intuitionistic Fuzzy divergence IF-D & Frequency ratio FR). The landslide susceptibility mapping is conducted using landslide inventory data and twelve conditional factors. The landslide susceptibility maps obtained from the two statistical models were compared with those generated by two deep machine learning models based on prediction accuracy measures, such as the Area Under the Curve (AUC) and Seed Cell Area Index (SCAI). The Success Rate Curve (SRC) was obtained using the training dataset, and the AUC values for the four models were as follows: 76.9% for IF-D, 76.9% for FR, 80.4% for DeeplabV3$^+$, and 76.3% for U-Net. In terms of the Prediction Rate Curve (PRC) obtained from the validation dataset, the AUC values were found to be 80.8% for IF-D, 80.8% for FR, 81% for DeeplabV3$^+$, and 77.8% for U-Net. To assess the classification ability of the models, the Seed Cell Area Index (SCAI) test was conducted. The results indicated that the SCAI (D-value) was 7.3 for U-Net, 10 for DeeplabV3$^+$, 7.6 for IF-D, and 9.1 for FR. Overall, the findings revealed that DeeplabV3$^+$ exhibited the highest prediction accuracy and classification ability, making it the most suitable choice for landslide susceptibility mapping in the relevant study area.

INTRODUCTION

Landslides are widely recognized as the most common and devastating geohazards in mountainous regions (Panchal & Shrivastava, 2022), significantly impacting both socioeconomic factors and human lives (Panahi et al. 2022). The occurrence and severity of landslides have been on the rise globally, attributed to the influences of climate change and human activities (Sajadi et al. 2022). Various factors contribute to these events, including frequent earthquakes, human activities such as road expansion on steep slopes, volcanic activities, and prolonged rainfall (Youssef & Pourghasemi 2021). The Karakoram and Himalayan mountainous terrain in the extreme northern part of Pakistan is prone to numerous landslides. The frequent occurrence of landslides in these rugged terrains can be attributed to factors such as repeated seismic activity, highly weathered lithologies, unstable slopes, and human activities (Shafique et al. 2016). The presence of active thrust faults, fractured lithologies, exposed geomorphology, and unconsolidated glacial-fluvial moraine on steep slopes further contributes to the susceptibility of the area to landslides (Hewitt 1998). In recent years, the Hunza River watershed basin located within the Karakoram Mountain range has experienced frequent devastating landslides (Derbyshire 2001). In January 2010, an especially destructive landslide occurred in Attabad village in Upper Gojal, resulting in the loss of twenty lives, the destruction of over three hundred houses,

and the formation of a new natural lake that persists to this day (Kargel et al. 2010). To address these natural hazards, landslide susceptibility maps can prove to be valuable tools for identifying areas vulnerable to landslides (Youssef & Pourghasemi 2021). These maps can be developed by considering various geo-environmental factors, including lithology, geomorphology, soil types, human activities, and drainage patterns.

Several approaches have been proposed for studying landslide susceptibility mapping, driven by advancements in computer science technologies and the availability of geospatial data. Many of these approaches utilize remote sensing data and Geographic Information Systems (GIS) (Chang et al. 2020). However, these methods often require extensive preparation related to landslides, including environmental, pedagogical, physical, geomorphological, and topographic considerations, as well as considerable knowledge and determination. Traditional approaches to landslide modeling rely on field excursions, which can be costly, site-specific, and time-consuming. Consequently, in the past few decades, statistical approaches for landslide susceptibility modeling have gained popularity (Al-Najjar & Pradhan 2021).

In general, landslide susceptibility mapping approaches encompass objective quantitative methodologies based on mathematical analysis, as well as qualitative methodologies involving subjective expert judgment (Bopche & Rege 2022). The heuristic technique involves the creation of susceptibility classes by assessing the relative contribution of landslide conditional factors to landslide formation (Dahal et al. 2008). The main limitation of heuristic methods, which fall under the qualitative approach, is the subjective nature of susceptibility assessments. On the other hand, the quantitative approach allows for the evaluation of the statistical relationship between the spatial distribution of known landslides and conditional factors (Chen et al. 2019). However, among the various landslide susceptibility techniques available, statistical approaches have gained popularity due to their accuracy and reliability in addressing the challenges of large-scale landslide mapping.

These methods can be categorized into qualitative, semi-qualitative, and quantitative approaches. The availability of remote sensing data, including topography and land cover information, has greatly facilitated the application of these techniques at large scales (Al-Najjar & Pradhan 2021). In recent years, researchers have extensively evaluated and applied various statistical models for landslide susceptibility analysis. These models include the Weight of Evidence (WOE) (Bopche & Rege 2022), Entropy Index (IOE) (Mondal & Mandal 2019), Support Vector Machine (Pandey et al. 2020), Neural Network (Abbaszadeh Shahri et al. 2019), Decision Tree methods (Wu et al. 2020), and Logistic Regression (Shan et al. 2020). However, each landslide susceptibility mapping (LSM) model has its advantages and disadvantages. It is common for different models to yield diverse evaluation outcomes when applied in the same region. To address these differences in prediction accuracies, many researchers have opted for multi-LSM models and conducted comparative analyses (Chen et al. 2019).

In recent years, various machine learning techniques (MLTs) have been utilized for tasks such as landslide susceptibility mapping, debris classification, and glacier lake mapping. Specifically, for landslide susceptibility mapping, several MLT techniques have been applied, including Artificial Neural Network (Youssef & Pourghasemi 2021), Support Vector Machine (X. Zhang et al. 2019), Decision Tree (Dou et al. 2019), and Random Forest (RF) (Sun et al. 2021).

Landslide occurrences depend on multiple factors (Zhang et al. 2019), including man-made activities, geomorphological conditions, weathering conditions, and others. While some factors can only be analyzed using qualitative or semi-qualitative methods (Zhang et al. 2021), there is inherent uncertainty in the landslide system (Zou & Xiao 2008). Fuzzy mathematical methods have been widely applied for landslide assessment to capture the complexity of these factors (Zhang et al. 2012). However, in classical fuzzy methods, the fuzzy nature is only represented by the membership function, whereas in intuitionistic fuzzy sets, the non-membership function is introduced to further explain the fuzzy concept (Zhang et al. 2021).

With the advancement of fuzzy set theory, various fuzzy models have been widely applied in various decision-making scenarios (Gu & He 2021). In the context of landslide susceptibility mapping, several entropy models and fuzzy models have been employed in landslide-prone areas. These include Shannon entropy (SE) (Nohani et al. 2019), index of entropy (IE) (Pourghasemi et al. 2012), Renyi divergence (RI) (Qin et al. 2001), intuitionistic fuzzy Jensen-Renyi divergence (IFJ-D) (Verma & Sharma, 2013), fuzzy gamma ray operator and AHP (Bera et al. 2019), and intuitionistic fuzzy set (Gu et al. 2022).

The concept of intuitionistic fuzzy sets, developed by Atanassov (1986), incorporates the degree of membership and non-membership functions with hesitancy such that their sum equals 1. Various modifications have been made to the classical fuzzy divergence model, with the latest version of modification being the Jensen-Renyi divergence. In the context of intuitionistic fuzzy sets, the Jensen-Renyi divergence is referred to as the Intuitionistic Fuzzy Jensen-

Renyi Divergence (IFJRD). This divergence provides more precise results than previous models, particularly in decision-making problems. However, it involves lengthy calculations and may fail for certain pattern sets (Verma & Sharma 2013).

In this study, the author introduces a refined fuzzy model, IF-D, derived from the intuitionistic fuzzy Jensen-Renyi divergence. This model streamlines computations and enhances performance on pattern sets. IF-D leverages original data effectively, employing straightforward mathematical calculations for probability analysis, resulting in superior accuracy compared to conventional models. Additionally, this research also aims to evaluate the efficacy of IF-D and classical models in landslide susceptibility mapping, focusing on classification capabilities and prediction accuracies. Furthermore, the study seeks to assess the accuracy, reliability, and suitability of deep machine learning techniques and statistical methods through a comparative analysis in the study area.

Study Area

Hunza watershed basin in the Karakoram mountainous range is in the Northern part of Pakistan. This watershed basin is fenced by the world's highest mountain ranges, i.e., Karakoram, Hindu-Kush, and the Himalayas. These mountain ranges comprise the world's highest and steep slopes with more than 45° slopes. The geographical location of the study area falls between the latitudes of 36°51'38.359" N, 35°55'22.231" N and longitudes of 76°0'45.354" E, 73°59'26.466" E. The elevation ranges from 1746 m to 7315 m above sea level. This watershed basin covers an area of 14305.07 km^2.

In Pakistan, particularly in the Karakoram mountainous range, landslides pose a common and significant threat to settlement areas (Ahmed et al. 2019). The study area, Hunza watershed basin, is situated in the Northern Karakoram Range of Pakistan (Fig. 1). The area is traversed by the Karakoram Highway (KKH), which serves as the primary trade and transportation route between China and Pakistan and has experienced numerous large-scale landslides in the past. The geomorphology of the study area is diverse, encompassing glacial-fluvial terraces, ancient moraines, loose material on steep scree slopes, debris fans, colluvium deposits, and talus deposits at the base of high cliffs (Hewitt 1998). The study area is characterized by a unique geology known as the Karakoram block. This block originated from the pre-Gondwanan supercontinent and drifted away during the late Paleozoic era before colliding with the Indian plate. The Hunza watershed basin is situated between two regional thrust faults: the Shyok Suture Zone to the south (Searle & Tirrul 1991) and the Rushan-Pshart Suture to the north (Pashkov & Shvol'man 1979).

Consequently, the rocks in the area are highly fragile due to the intense tectonic compressional regime, making the slopes highly susceptible to landslides exacerbated by frequent earthquakes. The Hunza River watershed covers an area of 13,571 km^2 and is nourished by some of the highest glaciers in the region. The Hunza River originates from this basin, serving as the starting point of the Indus River. The Indus River begins at the Khunjerab Pass and passes through the Hunza watershed basin, which is characterized by a network of long valley glaciers. See Fig. 1.

MATERIALS AND METHODS

The research methodology employed in this study involves seven main steps. (1) a detailed landslide inventory map of the study area is constructed by utilizing previous records, satellite imagery, and thorough field investigations. This map serves as the foundational map for data analysis, capturing the spatial distribution and occurrences of landslides in the study area. (2) twelve landslide conditional factors, including Slope, Aspect, Curvature, Geology, Distance to Fault, Distance to River, Distance to Road, Land cover, Topographic Wetness Index, Stream Power Index, and rainfall data, are selected through comprehensive field surveys of the study area. (3) Weight estimations of statistical models are analyzed to identify the spatial relationship between landslide conditional factors and landslide occurrence. (4) The landslide susceptibility maps are prepared using three state-of-the-art deep machine-learning techniques and statistical models. (5) The susceptibility maps generated from the machine learning techniques undergo validation using metrics such as F1 Score, Confusion Matrix, Precision, and IOU curve. (6) The landslide susceptibility maps produced from all four models are analyzed using the AUC (Area Under the Curve) and Seed Cell Area Index (SCAI). (7) A comparative analysis is conducted based on the results obtained from the models to determine their suitability and applicability for the specific study area, see Fig. 2.

Landslide Inventory Map

A global-scale landslide inventory was introduced by the International Geotechnical Societies' UNESCO Working Party on the World Landslide Inventory (deLugt & Cruden 1990). This inventory was later integrated into a database management system (Brown 1992). Mapping the spatial distribution of landslides is considered crucial before studying the relationship between landslide occurrence and its conditional factors, as highlighted by (van Westen et al. 1997). Various approaches, such as satellite images, aerial

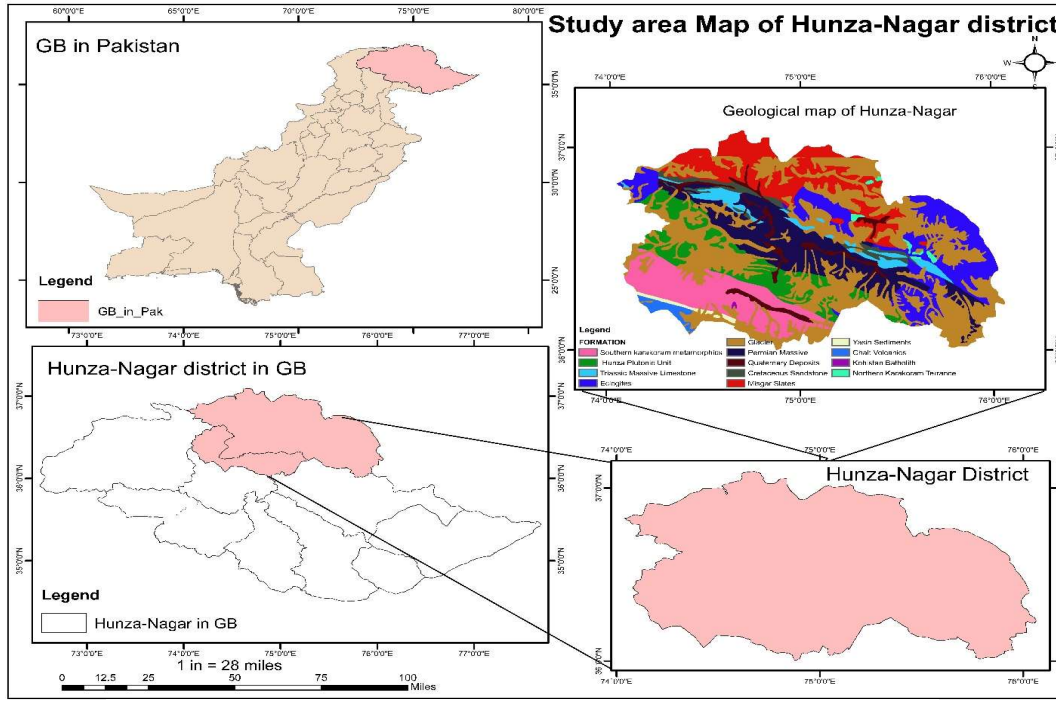

Fig. 1: Study area map, showing demographic boundaries and geological of area.

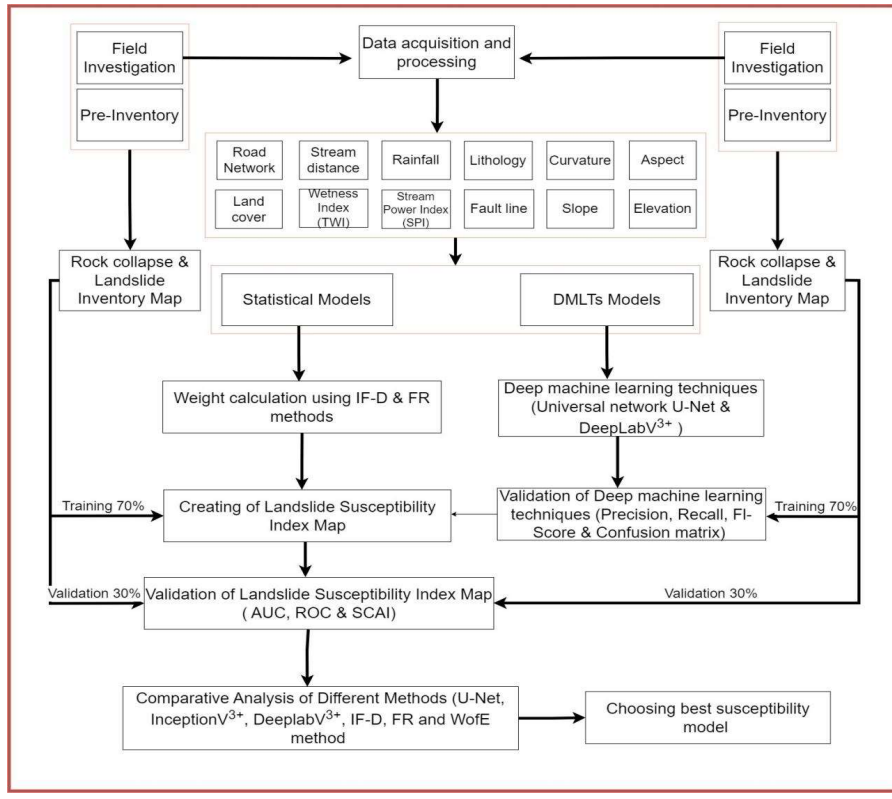

Fig. 2: Schematic flow chart for the adopted methodology.

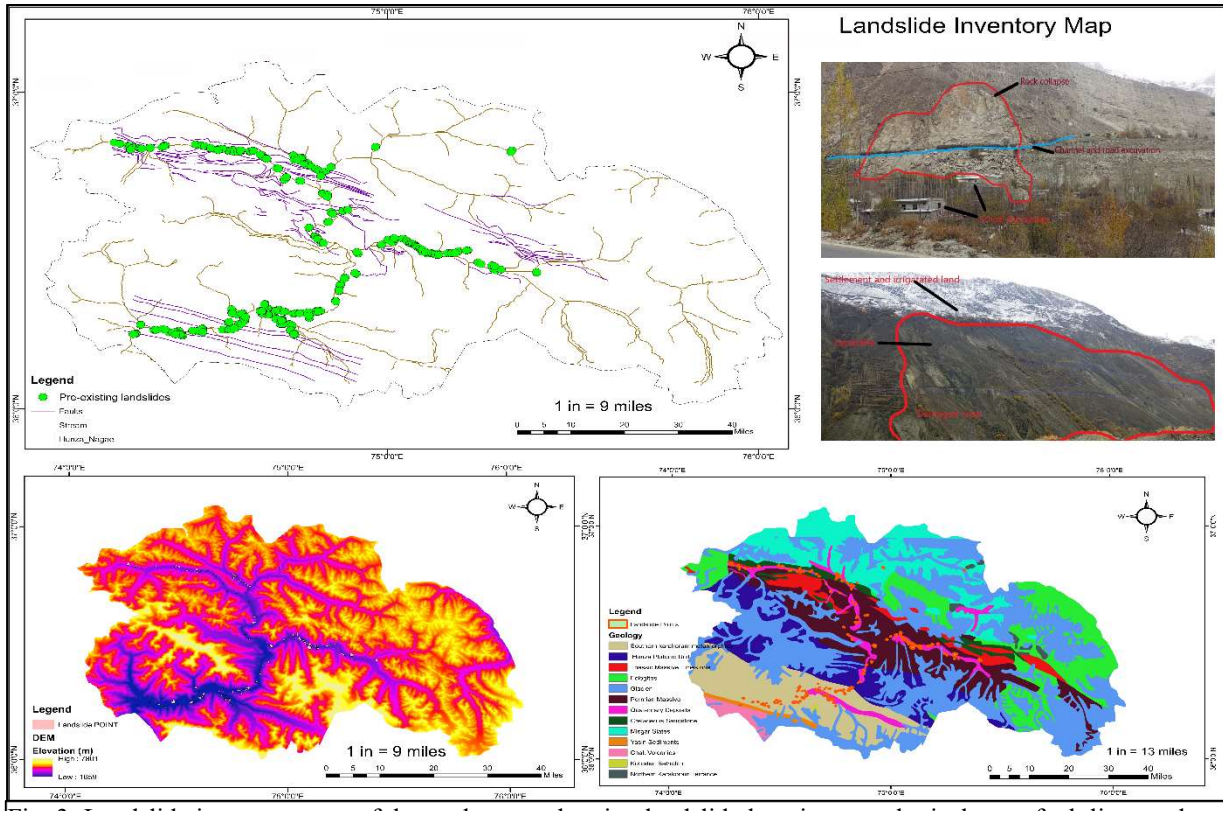

Fig. 3: Landslide inventory map of the study area, showing landslide locations, geological map, fault lines and some of the pictures of existing landslides.

photographs, and digital representations of topographic surfaces, can be used to map and identify landslides (Guzzetti, 2000). Therefore, landslide inventory maps play a vital role in regional landslide susceptibility mapping (Yan et al. 2019).

In this study, a comprehensive approach was employed, which involved the interpretation of aerial photographs, satellite images, earlier reports, and meticulous field investigations. Geologists and subject specialists were involved in the precise identification and marking of landslide sites. A total of 148 landslides were identified and marked in the study area using Garmin GPS with an accuracy of 3m. See Fig. 3 inventory map of the study area.

Landslide Conditional Factors

Landslide conditional factors are temporally and spatially dependent on the geomorphology of the study area. According to Yan et al. (2019), understanding the factors influencing landslide occurrences is crucial for landslide susceptibility mapping. Many researchers have conducted extensive investigations to identify the factors contributing to landslides and construct landslide susceptibility maps. These events are influenced by a combination of topographic, hydrological, and geological factors (Dou et al. 2019). The quality of landslide susceptibility maps relies not only on the selected models but also on the quality of the input data (Pourghasemi et al. 2013). Hong et al. (2016) emphasize that the selection of landslide conditioning factors is a key step in evaluating and mapping landslide susceptibility, as it directly impacts the quality of the resulting models. Based on the available literature, prior knowledge of landslide occurrence characteristics in the Hunza watershed basin, and the data availability for the study area, twelve landslide conditional factors were selected: slope, slope curvature, elevation, aspect, lithology, distance to faults, distance to rivers, distance to roads, topographic wetness index TWI), stream power index (SPI), land cover, and rainfall. All the thematic layer maps are shown in Fig. 4.

LSM Applying (DeeplabV3^{+})

DeeplabV3^{+} is the latest state of art machine learning model that has an encoder-decoder-based network for semantic segmentation. The DeeplabV3^{+} has a setup of deeplabV3 architecture as an encoder at the backup of ResNet. The architecture is divided into three parts: the encoder used for

feature extraction, ASPP to convert them into a wide scale information, and the encoder part arrayed to recuperate the spatial information. The extracted features in the encoder level are bilinearly up-sampled and then finally concatenated with the respective low-level features in the subsequent stage.

This model is built on the conception of Atrous Convolution and Atrous Spatial Pyramid Pooling (ASSP). In the Atrous convolution, the active field of view of the convolution is governed by a rate parameter. This Atrous convolution can be generalized as follows.

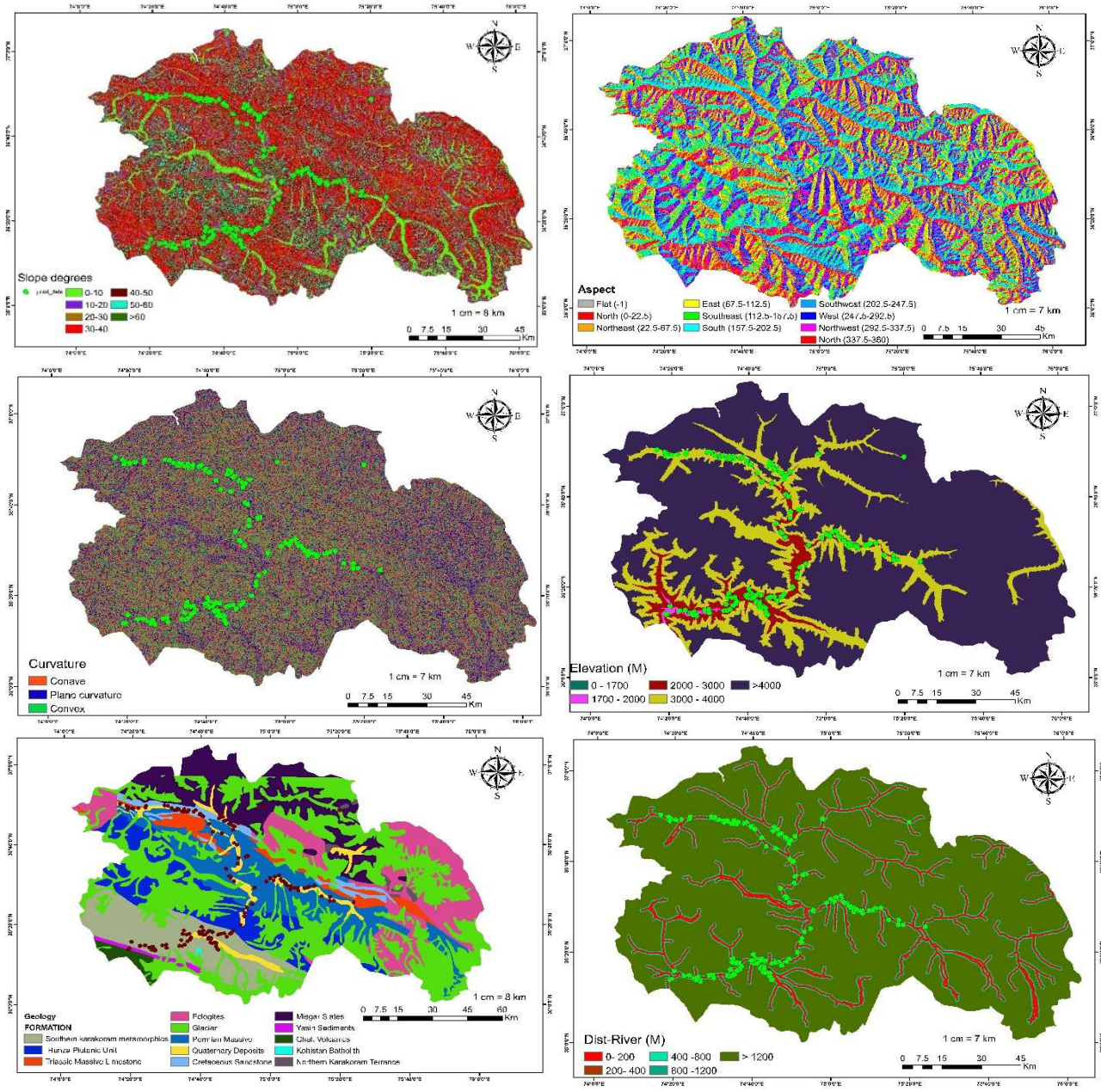

Figure Cont....

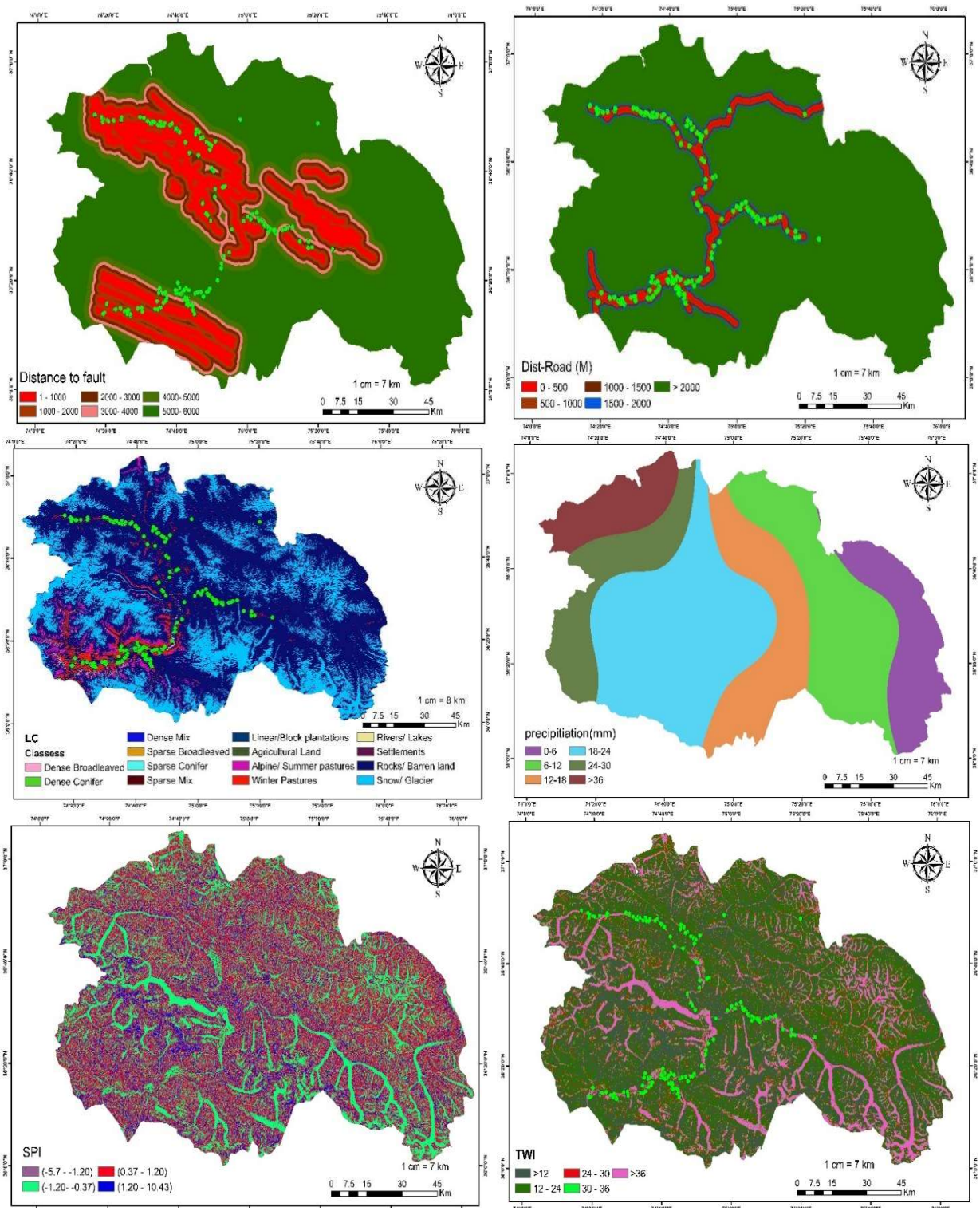

Fig. 4: Thematic layers of all 12 landslides conditional factors, the thematic layers have been classified into various classes for the probability analysis, the 12 landslide conditional factors are slope, aspect, curvature, elevation, distance to fault, distance to river, distance to road, land cover, topographic wetness index, stream power index, lithology and precipitation.

$$y[i] = \sum_{k} x\ [i + r\ .k]w[k]$$

Where w represents the filter, *i* denotes each location of output y, x is the input feature map, and r denotes the Atrous rate.

To regain information on different scales, several Atrous convolution layers can be applied. The ASPP can detain multi-scale data more capably with enormous Atrous rates. Thus DeeplabV3^{+} works as an encoder and depicts useful features at capricious resolution. Moreover, the ASPP can discover the convolutional features at several scales with multi-dilation rates. Therefore, better semantic information can be obtained from the output feature map of the encoder networks, which often contain 256 channels and are 32 times smaller than the resolution of the input image.

LSM Applying (U-Net)

U-Net is a deep machine-learning model that is useful for semantic segmentation purposes (Ronneberger et al. 2015). The architecture of the model has been modified to enable precise segmentation of targets even with limited training samples. U-Net has demonstrated excellent performance in remote sensing and segmentation tasks. The model follows an encoder-decoder structure, where the encoder path primarily consists of two 3×3 convolutional layers followed by 2×2 max-pooling layers. The convolutional layers act as moving windows that traverse the image (Zhang et al. 2019). Typically, U-Net takes input images with three channels, but for landslide susceptibility mapping, we have 12 channels or bands representing the thematic layers of landslide conditional factors. Therefore, it is essential to add additional layers to accommodate the increased input channels. In our model, we use the ResNet34 architecture as the encoder, allowing the extraction of multi-scale features from the input remote sensing data. The max-pooling operation in the encoder down samples the data with a stride of 2.

In contrast, the up-sampling in the decoder part is achieved by increasing the spatial size by a factor of 2 using bilinear interpolation. For this study, we utilized pre-trained weights from the ImageNet dataset for our encoder. To enhance the model's performance and prevent overfitting, we incorporated additional convolutional layers, such as Batch Normalization layers and dropout layers, with a rate of 0.2. The last convolutional layer consists of 5 neurons, and all the convolutional layers employ the Rectified Linear Unit (ReLU) activation function. The final output layer uses the Softmax activation function, which assigns a probability to each pixel indicating its belonging to a particular class in the LSM.

LSM Applying (Frequency Ratio FR)

The FR (Frequency Ratio) model is a statistical analysis approach that considers the spatial distribution of landslides and their conditional factors (Yan et al. 2019). It examines the number of pixels affected by landslides in a specific study area. The FR method applies conditional probability, whereby a stronger relationship between landslides and their influencing factors exists when the landslide-to-factor ratio is higher. This approach is in line with the works of Lee and Talib (2005), Pourghasemi (2008), Karim et al. (2011a), and (Khan et al. 2022), who also considered each class of landslide conditional factors and their associated pixels in landslide susceptibility mapping.

To implement the FR model for each class of landslide conditional factors, a combination is established between the landslide inventory map and criterion map Karim et al. (2011a). Therefore, in the process of landslide susceptibility mapping, it is essential to consider each class of landslides, their causative and conditional factors, as well as associated pixels both with and without landslides (Mandal & Mondal 2019).

To calculate the frequency ratio for each class of all the data layers, a combined expression will be used by using the following statistical expression (Karim et al. 2011b). Eq. 1.

$$Fr_i = \frac{N_{Pix(Si)}/N_{Pix(N_I)}}{\sum Npix_{(s_i)}/\sum Npix_{(N_I)}} \quad \ldots(1)$$

$N_{Pix(Si)}$ The number of pixels contains slides in each class (*i*)

$N_{Pix(N_I)}$ The total number of pixels having class in the whole watershed area

$\sum Npix_{(s_i)}$ The total number of pixels containing landslide

$\sum Npix_{(N_I)}$ The total number of pixels in the whole watershed area

LSM Applying (Intuitionistic Fuzzy Divergence IF-D)

The concept of fuzzy logic, proposed by Zadeh (1965), is based on the idea that each element should belong to a set with a membership value ranging between 0 and 1. Fuzzy logic allows for dealing with uncertainties in data using the Interval-Valued Fuzzy Sets (IFS) theory, which has proven beneficial in various research fields due to its ability to handle imprecise analysis. In probability theory, statistical divergence measures are commonly employed to quantify the differences between two probability distributions, as seen in the works of Kullback and Leibler (1951) and Rao (1985).

One specific divergence measure used in IFSs is known as the Intuitionistic Fuzzy Jensen-Rényi divergence (IFJRD).

While this divergence provides precise results in decision-making problems compared to classical fuzzy models, it involves lengthy calculations and has limitations when applied to certain pattern sets (Verma & Sharma 2013). To address these limitations, a new model called Intuitionistic Fuzzy Divergence (IF-Divergence) has been proposed, which overcomes the limitations of the Fuzzy Jensen-Rényi divergence model and is based on simpler calculations. In this study, the proposed IF-Divergence model is applied for landslide susceptibility mapping and probability analysis.

The fuzzy membership values can be derived from various methods of normalization of the frequency ratio (Abedi Gheshlaghi & Feizizadeh 2017). In the present study, fuzzy membership values were normalized from information values.

Step 01:

Normalized the Intuitionistic Fuzzy Matrix $R = \left(r_{ij}\right)_{(n\times m)}$

$$\gamma_{ij}[\pi_{ij}, v_{ij}, \pi_{ij}] = \begin{matrix} d_{ij} & for\ stable\ pixels \\ d_{ij} & for\ non-stable\ pixel \end{matrix} \quad \ldots(2)$$

Step 02:

Find the Ideal Solution

$$A^* = \{(\mu_{1*}, \nu_{1*}, \pi_{1*}), (\mu_{2*}, \nu_{2*}, \pi_{2*}), \ldots, (\mu_{m*}, \nu_{m*}, \pi_{m*})\} \quad \ldots(3)$$

Where $i = 1, 2, \ldots, n$

$$(\mu_{*i}, \nu_{*i}, \pi_{*i}) = \left\{{}^{max}_{j}\mu_{ij}, {}^{min}_{j}\nu_{ij}, 1 - {}^{max}_{j}\mu_{ij}, 1 - {}^{min}_{j}\nu_{ij}\right\} \quad \ldots(4)$$

Step 03:

$$D_n(A_j, A^*) = \frac{1}{2|X|}\sum_{i=1}^{n}\left\{\left|\mu_{Aj}(x_i) - \mu_{A^*}(x_i)\right| + \left|\nu_{A_j}(x_i) - \nu_{A^*}(x_i)\right| + \left|\pi_{A_j}(x_i) - \pi_{A^*}(x_i)\right|\right\}^n \quad \ldots(5)$$

Where $n = 1, 2, \ldots$

Step 05:

$$S(A, B) = 1\text{-}Dn \quad \ldots(6)$$

RESULTS AND DISCUSSION

Weight Estimation Using (FR & IF-D)

In the investigation, all the conditional factors contributing to landslides were transformed into a binary pattern, indicating the presence or absence of landslides, using the FR and divergence values. For continuous data such as slope, elevation, distance to fault, distance to the river, and road distance, they were first classified into different classes, and weights were separately estimated using the FR and IF-D models. In the case of continuous data, cutoff values were determined using the IF-D model, where the influence of a factor class on landslide occurrence is no longer statistically significant. The IF-D model identifies these cutoff values by examining the intersection points of similarity and divergence, enabling multi-generalization for continuous data.

For categorical data such as lithology, land cover, precipitation, curvature, SPI, TWI, and aspect, they were converted into a binary pattern based on the calculated weights from the FR and IF-D models for each factor class. The weights derived from the FR and IF-D models were then used to interpret the importance of each class of landslide conditional factor on landslide occurrences.

Cumulative Weights Using FR and IF-D

The influence of slope gradient below 20° and intersection point below 50° indicates that there is no influence of landslides. Therefore, this indicates that the cutoff valve for the slope gradient is 50°. Additionally, the minimum value of divergence D=0 and maximum valve of S=1 for the slope gradient 30º-40º indicates the maximum probability of landslide occurrence. In the case of frequency ratio, the weighted value of FR=1.62 represents the maximum value indicating the maximum probability of landslide occurrence for the slope gradient between slope class 30º-40º slope degrees.

Cumulative weights of elevation: The influence of elevation range intersection point is between 0-1700 m. This indicates that there is no influence of elevation on landslides. moreover, below 4000 m, the range of membership values tends to a maximum. Therefore, the results indicate the cutoff valve is below 4000 m. However, the maximum values indicated by S=1 and minimum values D=0 for the range of 2000 to 3000 m indicate the maximum probability and maximum influence of elevation on landslide occurrence. Furthermore, the results reveal that the similar highest value for frequency ratio FR=10.16 is the maximum for the same range of 2000 to 3000 m. This reflects that the highest association of landslide occurrence and maximum influence of elevation on landslide occurrence is in the range of 2000 to 3000 m.

Cumulative weights of distance to fault: For IF-D weight estimation, the boundary and intersection point lie below 5000 m. This indicates the cutoff value is below 5000 m, and the influence of distance to fault on landslide occurrence is below 5000 m. The number of landsides is about 11% for the range of 4000-5000 m; therefore, the cutoff point lies below

5000 m. Additionally, the similarity remains maximum, and divergence remains minimum from the range of 0-5000 m for the distance of fault. The result showed that the maximum influence of distance to fault on landslide occurrence is between 0-5000 m. Similarly, for frequency ratio weight estimation, the ascending trend in FR values from FR=2.02-2.95 for the class starts from 0-4000 m; additionally, the maximum value of FR = 2.95 for the same range between 3000 to 4000 m indicates that the influence of distance to fault on landslide occurrence can be found from 0 to 4000 m but maximum influence reached at 4000 m.

Cumulative weights for distance to river. Moreover, the weight values evaluated from IF-D showed a precise estimation regarding the weight cutoff value, which is indicated by the support and boundary of membership values. The cutoff value indicated by the cross-section point at 800 m indicates that there is no influence of distance to the river on landslide occurrence. Additionally, the values of divergence are minimum, and the values of similarity maximum for the class ranges from 0-800, indicating the maximum probability of landslide and maximum influence of distance to river on landslide occurrence.

Cumulative weights for distance to road. Therefore, the results indicate the cutoff value for the distance is below 2000 m. Additionally, the maximum value of similarity and minimum value of divergence is between the ranges of 0-500, this reflects that the maximum probability of spatial association of landslide and the influence of distance to the road lies between 0-500 m. On the other hand, the frequency ratio value FR= 4.00 indicates the maximum influence of distance to the river on landslides is 0 to 500 m. But at the same time, there is a decreasing trend in FR values for the classes from 0-2000 m. The result indicates that the influence of road distance has a substantial role in the distance ranges from 0-2000 m.

Slope aspect: Moreover, the weights estimated from IF-D represent the maximum value of S=1, and the minimum value D=1 indicates the maximum probability of landslide occurrence for the class flat aspect. Similarly, for the frequency ratio FR, the highest value of FR=1.50, with the highest frequency ratio value representing the highest probability of landslide occurrence for the class flat (-1).

Lithology: In the case of IF-D weight values, the maximum value of indicated by southern Karakorum metamorphic, cretaceous sandstone, Permian massive, and quaternary deposits. The support and boundary of the membership and non-membership functions represent the maximum probability of landslide occurrence on these lithological units. In the case of the frequency ratio model, the weight value of (FR= 5.0) corresponds to quaternary deposits followed by (FR= 3.74) cretaceous sandstone and (FR=2.16) Permian massive rocks. This indicates the highest landslide susceptibility class in these geological rock formations. This is because of the tectonic disturbance and active fault movement of the Klik fault in the upper Hunza Gojal area.

Stream Power Index (SPI): The weight derived from intuitionistic fuzzy divergence, indicates that the maximum value of S=1 and minimum value of D=0 is at the class (–5.7 - –1.23). The result showed the maximum probability of landslide and the highest probability of the influence of SPI for this class on landslide occurrence. Similarly, for the frequency ratio weight calculations from statistical analysis, the highest value of frequency ratio (FR=1.57) represents the highest value for the same class (1.2-10.43), indicating the highest probability of landslide occurrences among other classes for SPI classes. ***Land cover (LC)*** For intuitionistic fuzzy divergence the minimum divergence value and similarity value indicated that the highest probability of landslide is on barren land. The study area is at a high altitude, the area lacks natural forest, and most of the slopes are barren, settlements and irrigated lands lie below the water channels. Therefore, most of the landslides in the study area are due to channel excavation. It is, therefore, the derived values indicate most of the probability of landslides occurring on barren land. Besides the highest weight positive, the weight calculations for the frequency ratio of the highest valve (FR=2.96) indicate the maximum landslide susceptibility refers to orchards. The agricultural activities in orchards in hilly areas made the slopes vulnerable and accelerated landslides. On the other hand, the second highest value of FR=1.36 also indicates the maximum probability of landslide susceptibility.

Topographic Wetness Index (TWI): Additionally, from the statistical analysis of Frequency ratio weight estimation, the results revealed that the highest frequency ratio valve (FR=1.12) with the highest value for the range below >12 indicates the most landslide occurrence for TWI. However, the weight estimation from IF-D showed that the probability of landslide occurrence is below >12 for the TWI factor. The descending trend of similarity and ascending trend in divergence reflect that the influence of TWI decreases with an increase in classes (Table 1).

Precipitation: In the case of the intuitionistic fuzzy divergence model, the similarity S=1 and divergence D=0 for the class 18-24 mm of precipitation indicates the maximum probability of landslides occurrence. However, 93% of landslides exist in this class for precipitation. Therefore, based on acquired data and weight values derived from IF-D, the highest probability of landslide and influence of

precipitation is between 18-24mm in the case of precipitation. From frequency weight estimation, the highest value of FR= 2.9 for the class ranges (18-24). The results indicated that the high susceptibility of landslide occurs is in the range of 18-24 (Table 1).

Validation and Construction of Landslide Index Maps

The machine learning models are sensitive to data within their desired range. In this research assessment, the dependent factors were expressed as a binary variable, representing landslides and non-landslides. Therefore, the landslide causal factors were normalized to a range of 0 to 1, where 0 indicates non-landslides and 1 indicates landslides. The normalized data of the conditional factors were used as input for the machine learning models. To address the issue of overfitting, the dataset was divided into 70:30 ratios. 70% of the dataset was randomly selected for training the models, while the remaining 30% was used for validating the performance of the models. It's important to note that both negative and positive data were equally considered to generate the landslide susceptibility map.

The machine learning models were implemented and trained using the KERAS Python programming framework. Once the models were trained and validated, the final outputs were extracted to a GIS environment to validate the landslide susceptibility map. The validation of the susceptibility maps was performed using metrics such as the AUC curve and SCAI values. Finally, the landslide susceptibility indices (LSIs) were reclassified into different susceptibility zones using the ArcGIS 10.2 environment.

Validation of DMLT Models Using IOU and Loss Curve

The validation and training data for the deeplabV3^{+} DMLT model provided insightful results. The IOU (Intersection over Union) and Loss curves were utilized to assess the model's performance. For the training dataset, the IOU curve started at 0.35 and steadily increased, reaching a value of 0.74. Similarly, for the validation data, the IOU curve began at 0.1 and progressively rose to 0.7. These results indicate that the model demonstrates good detection and prediction accuracy. Furthermore, the Loss curve results showed a validation value of approximately 0.25, which is considered ideal and suggests that the model possesses excellent prediction accuracy. See the graphical representation of IOU in Fig. 5.

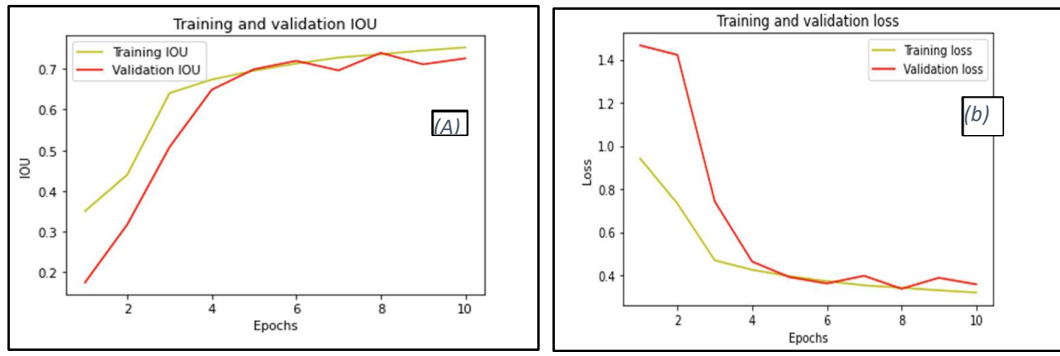

Fig. 5: IOU and loss curve for deeplabV3+, DMLTs. IOU (a), Loss curve (b).

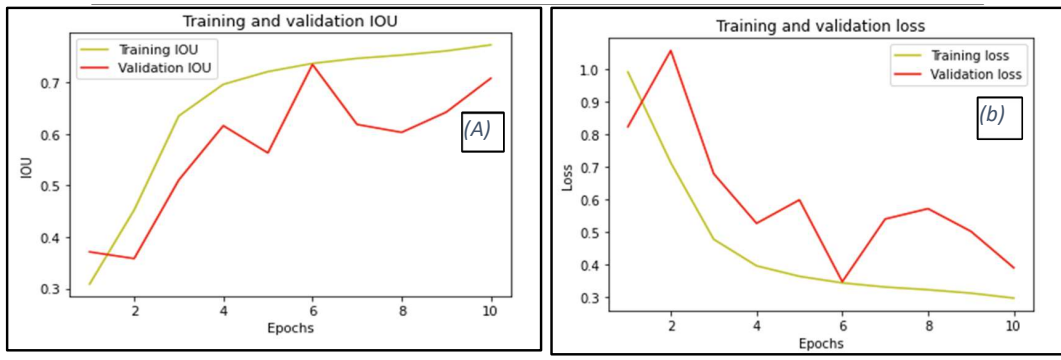

Fig. 6: IOU and Loss curve for U-Net, DMLTs. (a) IOU, (b), Loss curve.

Table 1: Weight estimation of all landslide conditional factors using bi-variate statistical models.

Factor	Classes	(STP) Stable Pixel	(LDP) Landslide Pixel	Intuitionistic Fuzzy Divergence (IF-D)			FR
				Hesitancy	Divergence (^1)	Similarity	FR
Slope	0-10	10673912	7963	0.9	0.6	0.4	0.0
	10-20	12222692	13645	0.8	0.5	0.5	0.4
	20-30	16617234	53055	0.6	0.3	0.7	1.1
	30-40	24525672	120091	0.3	0.0	1.0	1.6
	40-50	17540848	61826	0.6	0.3	0.7	1.2
	50-60	7842431	16212	0.9	0.6	0.4	0.7
	>60	2325655	3899	1.0	0.7	0.3	0.6
Aspect	Flat (-1)	810004	4559	1.0	0.0	1.0	1.9
	North (0-22.5)	6402821	28974	0.8	0.1	0.9	1.5
	Northeast (22.5-67.5)	12467219	47337	0.7	0.3	0.7	1.3
	East (67.5-112.5)	11039494	9454	0.8	0.1	0.9	0.3
	southeast (112.5-157.5)	11073594	19762	0.8	0.2	0.8	0.6
	South (157.5-202.5)	11541955	60733	0.7	0.3	0.7	1.7
	Southwest (202.5-247.5)	12256765	52173	0.7	0.3	0.7	1.4
	West (247.5-292.5)	10294776	19912	0.8	0.2	0.8	0.6
	Northwest (292.5-337.5)	10521353	17456	0.8	0.2	0.8	0.6
	North (337.5-360)	5340463	16331	0.9	0.0	1.0	1.0
Elevation	0-1700	6	0	1.0	0.5	0.5	0.0
	1700-2000	290915	6980	1.0	0.5	0.5	8.0
	2000-3000	4426712	135690	0.5	0.0	1.0	10.2
	3000-4000	16380340	131055	0.3	0.1	0.9	2.7
	>4000	70650471	2965	0.2	0.2	0.8	0.0
Curvature	Concave (-1.28- -0.001)	25940251	80636	0.0	0.1	0.9	1.0
	Flat (-0.001- 1.29)	55773965	171292	0.0	0.0	1.0	1.0
	Convex (1.29-88.32)	10034228	24762	0.1	0.3	0.7	0.8
Lithology	southern Karakoram metamorphic	9357596	70470	0.6	0.0	1.0	2.5
	Hunza plutonic unit	6146242	5614	0.9	0.3	0.7	0.3
	Triassic massive limestone	2582095	5946	1.0	0.3	0.7	0.8
	eclogites	10353152	0	0.9	0.3	0.7	0.0
	glacier	35163540	566	0.6	0.0	1.0	0.0
	Permian massive	10934340	71399	0.6	0.1	0.9	2.2
	quaternary deposits	2938134	94377	0.6	0.0	1.0	10.6
	cretaceous sandstone	1881467	21219	0.9	0.3	0.7	3.7
	Misgar slates	10143545	5383	0.9	0.2	0.8	0.2
	Yasin sediments	493283	633	1.0	0.4	0.6	0.4
	Chalt volcanic	884343	0	1.0	0.4	0.6	0.0
	Kohistan batholith	41605	0	1.0	0.4	0.6	0.0
	Northern Karakoram Terrance	435112	0	1.0	0.4	0.6	0.0

Table Cont….

...Cont. Table 1

Factor	Classes	(STP) Stable Pixel	(LDP) Landslide Pixel	Intuitionistic Fuzzy Divergence (IF-D)			FR
				Hesitancy	Divergence (^1)	Similarity	FR
Dist_Fault	0-1000	12345198	75160	0.6	0.0	1.0	2.0
	1000-2000	7116810	46309	0.8	0.1	0.9	2.2
	2000-3000	4813319	52215	0.8	0.1	0.9	3.6
	3000-4000	4390897	39129	0.8	0.0	1.0	3.0
	4000-5000	7474161	32764	0.8	0.0	1.0	1.5
	>5000	55608059	31113	0.3	0.5	0.5	0.2
Dist_River	0-200	4911209	38647	0.8	0.0	1.0	2.6
	200-400	4427540	62049	0.7	0.1	0.9	4.6
	400-600	4105746	57210	0.7	0.1	0.9	4.6
	600-800	3963514	45730	0.8	0.0	1.0	3.8
	>800	74340288	73054	-0.1	0.9	0.1	0.3
Dist_Road	0-500	2889524	129326	0.5	0.0	1.0	14.8
	500-1000	2402126	88376	0.7	0.2	0.8	12.2
	1000-1500	2287711	36399	0.8	0.3	0.7	5.3
	1500-2000	2214121	10905	0.9	0.4	0.6	1.6
	>2000	81954962	11684	0.1	0.4	0.6	0.0
SPI	(-5.7 - -1.20)	7395668	22606	0.8	0.0	1.0	1.0
	(-1.20 - 0.37)	31839391	55789	0.5	0.4	0.6	0.6
	(0.37 - 1.20)	38492081	131706	0.1	0.7	0.3	1.1
	(1.20 - 10.43)	14021304	66589	0.6	0.2	0.8	1.6
LC	Natural forest	342085	48	1.0	1.0	0.0	0.0
	Orchards	410062	3678	1.0	1.0	0.0	3.0
	Agriculture land	199084	623	1.0	1.0	0.0	1.0
	Summer Pasture	2399038	2649	1.0	1.0	0.0	0.4
	Winter Pasture	2244705	16382	0.9	0.9	0.1	2.4
	River/Lakes	113378	33	1.0	1.0	0.0	0.1
	Settlements	27535	124	1.0	1.0	0.0	1.5
	Barren land	61298772	253131	-0.6	0.0	1.0	1.4
	Snow/Glacier	24189260	22	0.7	0.7	0.3	0.0
Precipitation	>6	10679048	0	0.9	1.1	-0.1	0.0
	6 - 12	19270617	9081	0.8	1.0	0.0	0.1
	12-18	14131172	29114	0.8	1.0	0.0	0.3
	18 - 24	29012457	565691	-0.3	0.0	1.0	2.9
	24 - 30	10731572	2271	0.9	1.1	-0.1	0.0
	30-36	7153291	0	0.9	1.2	-0.2	0.0
TWI	>12	78961564	267502	-0.8	0.0	1.0	1.1
	12- 24	7237810	3186	0.9	0.9	0.1	0.1
	24- 36	2559283	713	1.0	1.0	0.0	0.1
	36-48	614958	165	1.0	1.0	0.0	0.1
	>48	2374829	5124	1.0	1.0	0.0	0.7

Fig. 5 showcases the validation of the U-Net model using 70% of the training dataset for 10 epochs. The IOU curve displayed an initial value of 0.3, eventually reaching 0.79. Likewise, the IOU value of 0.69 for the 30% validation dataset indicates good prediction accuracy and alignment with the ground truth. Additionally, the Loss curve validation for the U-Net model yielded a value of 0.4, further affirming the model's reliable prediction accuracy. See Fig. 6. Overall, the IOU and Loss curves demonstrate that both the deeplabV3$^+$ and U-Net models exhibit excellent detection and prediction accuracy.

Validation of DMLT Models Using Confusion Matrix

The confusion matrix is an N*N matrix that evaluates the classification performance of the ML model. In the confusion matrix, the matrix compares the actual target values with predicted values by machine learning technique for a given set of data. In ML, a good model is with those high true positive and true negative rates. Additionally, in this study, three DML models were also validated based on the scores of the confusion matrix. The results showed that the three ML models have good classification performance in landslide detection for the given data set. see Fig. 7.

Validation of DMLT Models Using Recall, Precision and F1 Score

Based on the comparative assessment of the three executed models, namely DeeplabV3+ and U-Net, the results indicate favorable performance for classification in the relevant study area. For both the DeeplabV3$^+$ and U-Net models, the precision and recall values were found to be 0.85 and 0.89, respectively. These results suggest that all the models performed well and exhibited good classification abilities.

The F1 score is a crucial evaluation metric used to validate the models' performance. It combines multiple competing metrics to provide an overall assessment of the model's analytical performance. In machine learning, an F1 score of 1 represents a perfect score, while a score of 0 signifies model failure. In the case of the three executed DMLTs models, the results revealed that DeeplabV3+ achieved an F1 score of 0.89 and an accuracy of 0.8, while U-Net attained an F1 score of 0.89. These findings indicate that both DMLT models exhibited satisfactory performance based on their F1 scores and accuracy. Overall, the comparative assessment demonstrates that the DeeplabV3$^+$ and U-Net models performed well as classifiers, showcasing their effectiveness in the classification task for the specific study area. See Fig. 8.

Validation Landslide Susceptibility Index Maps Based on AUROC

According to Fabbri and Chung (2019), validating the performance of a model requires splitting the dataset into separate subsets. In this study, particularly the dataset was divided into two sets for validation and prediction of susceptibility maps. However, no specific criteria were applied for the selection of the splitting datasets (Pradhan 2013). The dataset was divided into a 30:70 ratio, where 30% of the dataset was used for validation and 70% for model building, also known as the training dataset. This validation method has been commonly employed in previous studies (Suzen & Doyuran 2004, Zhang et al. 2019).

The area under the ROC curve (AUC) values are utilized to assess the accuracy, often referred to as the "prediction rate," of the models. The AUC value ranges from 0.5, indicating random prediction represented by the diagonal reference line, to 1, representing perfect prediction (Huang

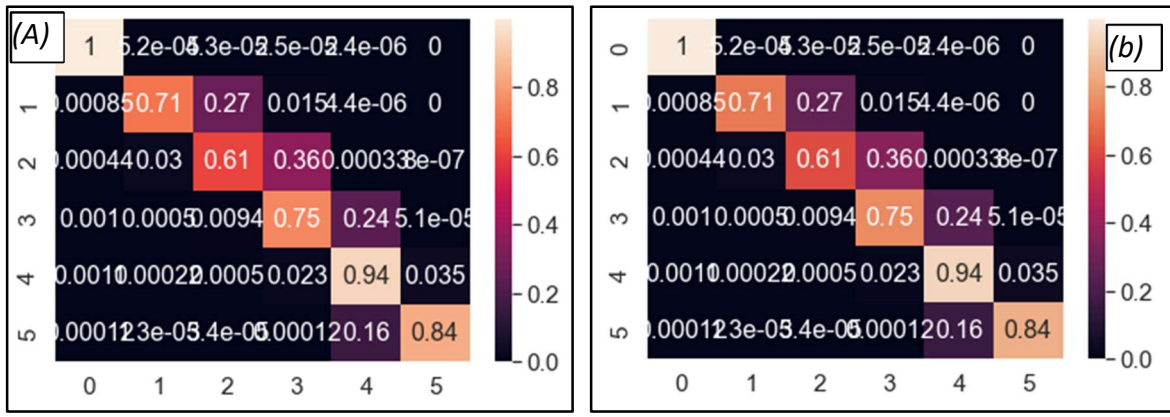

Fig. 7: Confusion matrix, deeplabV3+ (A) and U-Net (b).

(a)

	precision	recall	f1-score	support
0	1.00	1.00	1.00	27461588
1	0.96	0.71	0.82	3837326
2	0.67	0.61	0.64	3760218
3	0.82	0.75	0.78	9709555
4	0.77	0.94	0.84	9895272
5	0.89	0.84	0.86	3218665
accuracy			0.89	57882624
macro avg	0.85	0.81	0.82	57882624
weighted avg	0.90	0.89	0.89	57882624

(b)

	precision	recall	f1-score	support
0	1.00	1.00	1.00	27461588
1	0.96	0.71	0.82	3837326
2	0.67	0.61	0.64	3760218
3	0.82	0.75	0.78	9709555
4	0.77	0.94	0.84	9895272
5	0.89	0.84	0.86	3218665
accuracy			0.89	57882624
macro avg	0.85	0.81	0.82	57882624
weighted avg	0.90	0.89	0.89	57882624

Fig. 8: Precision, recall and F1 scores for DeeplabV3+ (a), U-Net (b).

2012). An AUC value of 1 signifies a perfect model, while a value of 0.5 indicates incorrect models (Tien Bui et al. 2016). Overall, splitting the dataset for validation and utilizing the AUC values provide a means to evaluate the accuracy and performance of the models, as mentioned by Fabbri and Chung (2019) and supported by previous studies (Suzen & Doyuran, 2004, Zhang et al. 2019).

The ROC curve indicates the correlation between "Sensitivity and "Specificity, which are as follows:

$$\text{Sensitivity} = \frac{TP}{TP+F} \quad \ldots(7)$$

$$\text{Specificity} = \frac{TN}{FP+TN} \quad \ldots(8)$$

TP is a true positive rate, FN is a false-negative rate, TN is a true negative rate, and FP is a false positive rate.

For the training and validation of LSI for statistical models. The results indicated the success rate cure for FR was 81% and IF-D 81%. The result revealed from the prediction rate curve for FR 77% and IF-D 77%. The prediction accuracy for the three statistical models is satisfactory to estimate the newly proposed model IF-D performed well whose prediction accuracy is equal to FR. This concludes that the newly proposed model fits the landslide susceptibility mapping for the pertinent study area. See the graphical representation of the prediction and success rate cure in Fig. 9.

Validation of Landslide Index Maps Based on Seed Cell Area Index (SCAI)

The Seed cell area index (SCAI) (Suzen & Doyuran 2004) was used to estimate the differences between the divided zones for LSM models. In this study, SCAI was applied to evaluate the classification capabilities of four LSM models more precisely and also to identify the differences between the divided zones of LSM models. The best classifier could make large differences between the divided zones. Likewise, the lower difference between the divided zones indicates the

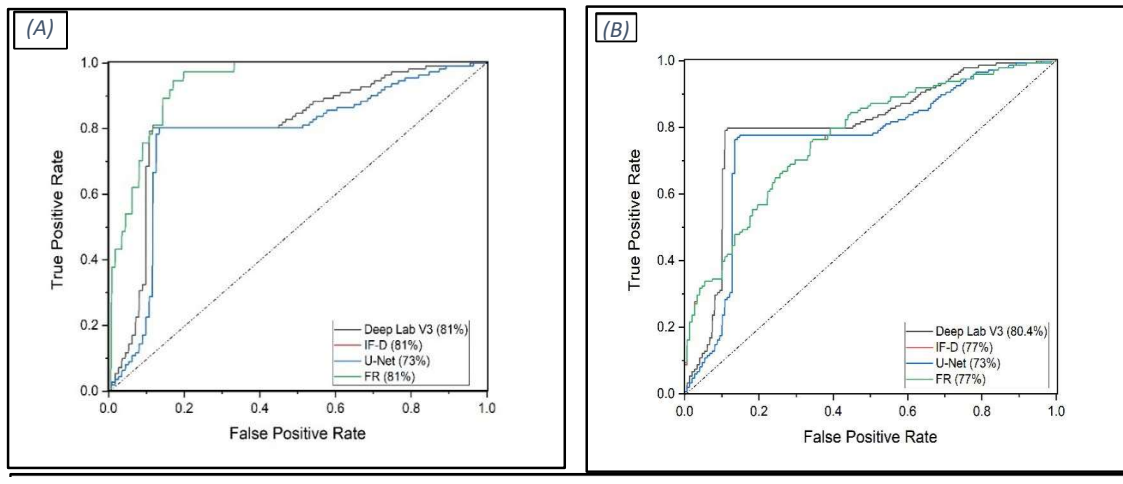

Fig. 9: Training and Validation of landslide susceptibility index maps based on AUROC. (a) Success Rate Curve (SRC) and (b) Prediction Rate Cure (PRC).

low classification capability of LSM. The landslide grid cell is called the "Seed cell," and the SCAI can be calculated using the following equation (Tang et al. 2021).

$$SCAI = \frac{\%\ Area}{\%\ seed} \quad \ldots(9)$$

Where $\%_{area}$ indicates the percentage of grid cells in each susceptibility class to total grid cells in the whole area, while $\%_{seed}$ Indicates the percentage of landslide grid cells in each susceptibility class to grid cells of all landslides. The values of SCAI represent the proneness of landslide. The higher value of SCAI shows the low- proneness of the landslide, while the low value of SCAI indicates the high proneness of the landslide. Similarly, the Differential value (D-value) represents the difference in SCAI for each susceptibility zone. The higher difference in D-value is the low proneness of the landslide, and the lower difference in D-value, the higher proneness of landslide probability. The higher value of SCAI shows the low- proneness of the landslide, while the low value of SCAI indicates a high proneness of the landslide.

Additionally, the difference in SCAI indicated by D-Value between low and very high for DeeplabV3$^+$ is 672, U-Net 7.34, IF-D 7.6, and FR 9.1. The result indicates deeplabV3$^+$ D=6.7 showed that the model has the highest accuracy of classification capability among the other three models. See Table 2.

DISCUSSION

In general, the evaluation of landslide occurrences involves analyzing past landslide events caused by predisposing factors, which serves as a guideline for predicting future landslides. This connection between landslide occurrence and the underlying conditional factors can be identified. In this regard, intuitionistic fuzzy divergence provides a means to assess the relationship and membership among factor classes. The models also offer insights into the influence of conditional factors on landslide occurrences through similarity and divergence values. The present study aimed to assess landslide susceptibility models (LSMs) and weight estimation using Intuitionistic Fuzzy Divergence (IF-D) in comparison with Frequency Ratio (FR). The susceptibility maps generated were based on a pixel-based analysis of twelve landslide conditional factors that contribute to the level of landslide susceptibility. Moreover, the weights assigned to each geo-environmental factor for each class were objectively determined through a precise mathematical solution using intuitionistic fuzzy divergence, and these weights were compared to those derived from the frequency ratio model.

Moreover, this study evaluates the performance of two statistical models (FR and IF-D) and two deep machine learning models (U-Net and DeeplabV3$^+$) for landslide susceptibility mapping (LSM) in the Hunza watershed basin of Northern Pakistan. The utilization of remote sensing, GIS, and Karas Python programming proved beneficial in developing a spatial database for susceptibility analysis. This research contributes to understanding the spatial contribution of landslide factors and predicting landslide susceptibility values for specific geographic locations. Previous studies

Table 2: Results of Seed Cell Area Index (SCAI) for all four statistical LSM models.

LSM Models	Class	Total no of Pixel	% Area	No Landslide Pixels	Seed %	SCAI	D-Value
U-Net	Very high	45961427	50.1	199003	71.9	0.7	
	High	26921671	29.4	63016	22.8	1.3	0.6
	Moderate	10268183	11.2	11467	4.1	2.7	1.4
	Low	8527751	9.3	3202	1.2	8.0	5.3
DeepLabV3$^+$	Very high	40185752	43.8	201751	72.9	0.6	
	High	29521577	32.2	61660	22.3	1.4	0.8
	Moderate	10902779	11.9	10095	3.6	3.3	1.8
	Low	11137190	12.1	3156	1.1	8.0	5.0
IF-D	Very high	16447576	18.4	124273	44.9	0.4	
	High	62105787	69.4	147914	53.5	1.3	0.9
	Moderate	10890117	12.2	4502	1.6	7.5	6.2
	Low	34356	0.0	1	0.0	8.0	0.5
FR	Very high	16447576	18.4	124273	44.9	0.4	
	High	62105787	69.4	147914	53.5	1.3	0.9
	Moderate	10890117	12.2	4502	1.6	7.5	6.2
	Low	34356	0.0	1	0.0	9.5	2.0

have indicated that slopes with degrees between 30 and 50 are more prone to landslides in the region, while slopes greater than 50 degrees have a lower influence on landslide susceptibility (Bacha et al. 2018). The findings of this research align with these previous studies, particularly with the slope of the study area.

Furthermore, regarding the slope gradient, the weights derived from IF-D (with minimum D-0, S=1) and the maximum value of FR (1.62) indicate a higher probability of a spatial relationship between landslide occurrence and slopes ranging from 30-40 degrees. Similarly, for continuous data such as elevations, the results show that the maximum value of FR (10.16), S=1, and D=0 correspond to the class of elevations between 2000-3000 m, suggesting a spatial relationship with landslide occurrences. However, in the case of the influence of the river, the study reveals that the distance to the river does not perform well when using FR as a measure. It is evident that as the distance to the river decreases, the influence of the river on landslide occurrences increases. In the case of FR, the weight values follow an ascending order, indicating imprecise estimation. On the other hand, the weight values derived from IF-D provide a more accurate estimation of the influence of distance from the river on landslide occurrences. Specifically, for distances between 0-200 m, the divergence values exhibit an ascending order with D=0. See Table 2.

Faults play a significant role as conditional factors for landslides. In the study area, regional faults to the south and the local fault system to the north are the dominant factors contributing to landslide occurrences. The landslide inventory map of the study area confirms that most landslide clusters are concentrated in the northern and southern parts. The weight derived from the statistical analysis of IF-D indicates that most landslides occur within a circumference of 0-1000 m from the faults. The analysis also reveals that proximity to roads is a significant factor in destabilizing slope stability. Areas within a radius of 0-500 m from roads are more susceptible to landslides. Blasting for construction purposes has weakened slopes and made them vulnerable to landslides. In the construction of the Karakoram Highway, extensive blasting activities have contributed to slope instability in the region.

Furthermore, the weight values derived from FR do not precisely indicate the effect of faults on landslide occurrences. The valley in the study area predominantly follows an east-west direction, with slopes dipping towards the south and north. This topographical characteristic results in less natural vegetation, rendering the slopes more vulnerable to landslides. The slope aspect categories—Flat (FR=1.9, D=0.0), North (FR=1.5, D=0.1), and South (FR=1.7, D=0.3)—exhibit the highest probability of landslide occurrences in this terrain. Regarding categorical data such as geology, the weight values suggest that certain lithological units have a higher probability of landslide occurrence. The southern Karakoram metamorphic unit (FR=2.5, D=0.02), quaternary deposits (FR=10.6, D=0.00), Permian massive (FR=2.2, D=0.07), and cretaceous sandstone (FR=3.5, D=0.2) show the highest likelihood of landslides. These lithological units in the northern and southern parts of the study area are highly influenced by two major regional faults present in the north and south. Man-made activities play a crucial role in destabilizing slopes in the study area, as indicated by the maximum FR value of 3.0 for orchards, FR=2.4, D=0 for winter pastures, and FR=1.4, D=0 for barren land. These activities have altered the natural landscape, contributing to increased landslide susceptibility.

Deep machine learning techniques (DMLTs) have gained significant popularity in the scientific community for modeling various environmental phenomena, as they enable the exploration of complex relationships. In the context of landslide susceptibility analysis, several machine-learning techniques have been employed. In this study, the DeeplabV3$^+$ and U-Net models were utilized to assess landslide susceptibility in the Hunza watershed basin. The LSMs for the study area were developed using Python programming in the KARAS software environment and subsequently exported to GIS for final mapping. To address the issue of overfitting, a sampling ratio of 70% for training the model and 30% for validation was employed. The data was partitioned into 126/256 patches, and the model was trained for 10 epochs.

To comprehensively evaluate the training and validation of DMLT models, a wide range of state-of-the-art deep machine learning techniques were employed, utilizing accuracy statistics. Validation of the prediction map is crucial for assessing the implications of the results in landslide prediction modeling. Various validation tests, including the F1 score, IOU curve, and ACC score, were performed to validate the deep machine learning models (DMLTs). The validation results for IOU (0.74, 0.69) and the loss curve for DeeplabV3$^+$ and U-Net (0.25, 0.1) indicate excellent prediction accuracy for this study. Similarly, the precision and recall values (0.85, 0.89) for DeeplabV3$^+$ and U-Net suggest that both models are effective classifiers and demonstrate strong classification ability for the study area. After training and validating the models, landslide susceptibility maps were generated using DeepLabV3$^+$ and U-Net. These maps were categorized into distinct susceptibility classes, namely very high, high, medium, and low, within the GIS 10.2 environment. Furthermore, to produce LSMs

using IF-D and FR, parameter scores and FR values were combined from the respective parameter maps. These values were then aggregated from twelve scaled parameters within the ArcGIS 10.2 environment to obtain a landslide susceptibility map. The resulting LSI map from IF-D and FR was subsequently classified into four susceptibility zones Fig. 10.

To assess the goodness of fit and prediction accuracy of LSMs, this research utilized the AUC curve and Seed Cell Area Index (SCAI). The AUC curve was employed to generate the Success Rate Curve (SCR) and Prediction Rate Curve (PCR) using the training and validation datasets. Verification and testing of the LSMs' accuracy are crucial aspects that need to be addressed. In this study, we applied the Receiver Operating Characteristic (ROC) curve and calculated the Area Under the Curve (AUC). This validation method has been widely used in previous studies (Suzen & Doyuran, 2004, X. Zhang et al. 2019).

For the Prediction Rate Curve (PRC) obtained from the validation dataset, the AUC values were determined as 80.8% for IF-D, 80.8% for FR, 81% for DeeplabV3^{+}, and 77.8% for U-Net (refer to Fig. 9). To assess the classification ability of the models, the Seed Cell Area Index (SCAI) test was employed. See Table 2. The results indicated that the SCAI D-value was 7.3 for U-Net, 10 for DeeplabV3^{+}, 7.0 for IF-D, and 9.1 for FR.

Furthermore, the accuracy statistics revealed that the IF-D model exhibited 44.9% of landslides in the very high susceptibility zone and 53.5% in the high susceptibility class. Similarly, the percentage area of landslides was 44.8% for the very high susceptibility class and 53% for the high susceptibility class. Table 2.

CONCLUSIONS

Landslide susceptibility mapping plays a crucial role in reducing the risk of disasters in landslide-prone areas.

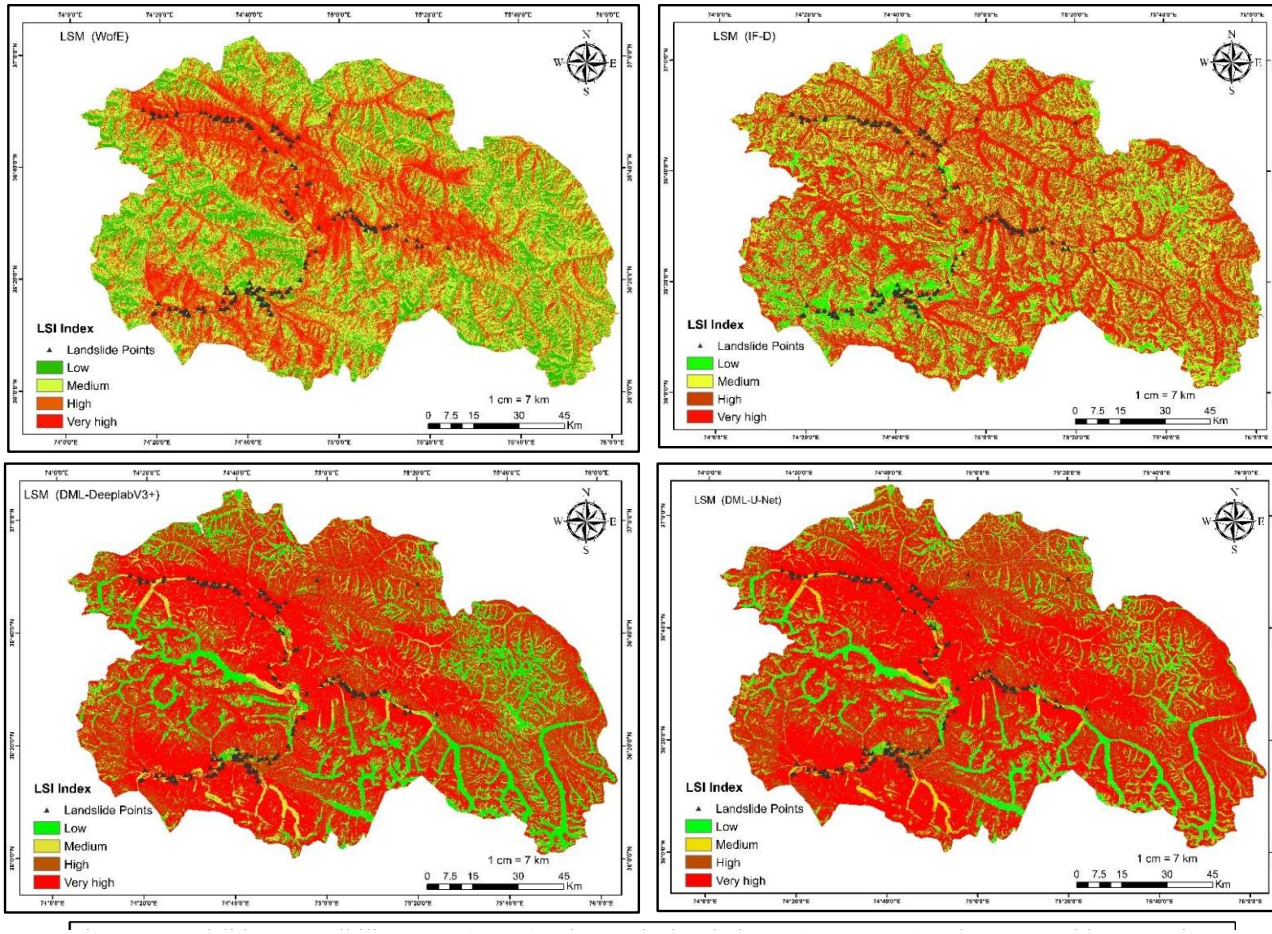

Fig. 10: Landslide susceptibility maps (LSMs) using statical techniques (IF-D & FR) and Deep Machine Learning models (DeeplabV3+& U-Net). Final susceptibility maps classified into four susceptibility zones.

This study focused on the Hunza watershed basin in northern Pakistan, which experiences frequent rockslides and landslides as geological phenomena. The occurrence of landslides is directly influenced by various conditional factors, and each factor class contributes differently to the modeling and mapping of the area. To assess the significance of each factor class in landslide occurrences, a proposed model and FR model were utilized. In terms of weight estimation for each conditional factor, the proposed model demonstrated greater reliability in identifying the spatial relationship of the conditional factors.

Two advanced deep machine learning techniques, DeeplabV3$^+$ and U-Net, along with two bi-variate statistical models, IF-D and FR, were executed to assess and map landslide susceptibility in the study area. The performance of these models was compared based on prediction accuracy, accuracy statistics, and SCAI. DeeplabV3$^+$ demonstrated a prediction accuracy of 80% and an SCAI of 7.6 D-value, making it the recommended choice for landslide susceptibility mapping in the study area.

REFERENCES

Abbaszadeh Shahri, A., Spross, J., Johansson, F. and Larsson, S., 2019. Landslide susceptibility hazard map in southwest Sweden using artificial neural network. *CATENA*, 183, p.4225. https://doi.org/10.1016/j.catena.2019.104225.

Abedi Gheshlaghi, H. and Feizizadeh, B., 2017. An integrated approach of analytical network process and fuzzy-based spatial decision-making systems applied to landslide risk mapping. *Journal of African Earth Sciences*, 133, pp.15–24. https://doi.org/10.1016/j.jafrearsci.2017.05.007.

Ahmed, M.F., Ali, M.Z., Rogers, J.D. and Khan, M.S., 2019. A study of knick point surveys and their likely association with landslides along the Hunza River longitudinal profile. *Environmental Earth Sciences*, 78(5), p. 176. https://doi.org/10.1007/s12665-019-8178-3.

Al-Najjar, H.A.H. and Pradhan, B., 2021. Spatial landslide susceptibility assessment using machine learning techniques assisted by additional data created with generative adversarial networks. *Geoscience Frontiers*, 12(2), pp. 625–637. https://doi.org/10.1016/j.gsf.2020.09.002.

Atanassov, K., 1986. Intuitionistic fuzzy sets. *Fuzzy Sets and Systems*, 20, pp. 87–96.

Bera, S., Guru, B. and V. R., 2019. Evaluation of landslide susceptibility models: A comparative study on the part of Western Ghat Region, India. *Remote Sensing Applications: Society and Environment*, 13, pp.39–52. https://doi.org/10.1016/j.rsase.2018.10.010.

Bopche, L. and Rege, P.P., 2022. Landslide susceptibility mapping: An integrated approach using geographic information value, remote sensing, and weight of evidence method. *Geotechnical and Geological Engineering*, 40(6), pp. 2935–2947. https://doi.org/10.1007/s10706-022-02070-4.

Brown, D., 1992. Ohmeda arkive1 patient information management system—an operating room-based database analysis network. In: Ikeda, K., Doi, M., Kazama, T., Sato, K. and Oyama, T. (eds.), *Computing and Monitoring in Anesthesia and Intensive Care*, Springer, pp. 201–202. https://doi.org/10.1007/978-4-431-68201-1_56.

Chang, Z., Du, Z., Zhang, F., Huang, F., Chen, J., Li, W. and Guo, Z., 2020. Landslide susceptibility prediction based on remote sensing images and GIS: Comparisons of supervised and unsupervised machine learning models. *Remote Sensing*, 12(3), p. 3. https://doi.org/10.3390/rs12030502.

Chen, W., Zhao, X., Shahabi, H., Shirzadi, A., Khosravi, K., Chai, H., Zhang, S., Zhang, L., Ma, J., Chen, Y., Wang, X., Bin Ahmad, B. and Li, R., 2019. Spatial prediction of landslide susceptibility by combining evidential belief function, logistic regression, and logistic model tree. *Geocarto International*, 34(11), pp. 1177–1201. https://doi.org/10.1080/10106049.2019.1588393.

Dahal, R.K., Hasegawa, S., Nonomura, A., Yamanaka, M., Dhakal, S. and Paudyal, P., 2008. Predictive modeling of rainfall-induced landslide hazard in the Lesser Himalayas of Nepal based on weights-of-evidence. *Geomorphology*, 102(3), pp. 496–510. https://doi.org/10.1016/j.geomorph.2008.05.041.

deLugt, J.S. and Cruden, D.M., 1990. The world landslide inventory. *Infrastructure Management, Transportation Public Safety, Land Records Modernization, Natural Resource Management*, 64, pp. 112–124.

Derbyshire, E., 2001. Geological hazards in loess terrain, with particular reference to the loess regions of China. *Earth-Science Reviews*, 54(1), pp. 231–260. https://doi.org/10.1016/S0012-8252(01)00050-2.

Dou, J., Yunus, A.P., Tien Bui, D., Merghadi, A., Sahana, M., Zhu, Z., Chen, C.-W., Khosravi, K., Yang, Y. and Pham, B.T., 2019. Assessment of advanced random forest and decision tree algorithms for modeling rainfall-induced landslide susceptibility in the Izu-Oshima Volcanic Island, Japan. *Science of The Total Environment*, 662, pp. 332–346. https://doi.org/10.1016/j.scitotenv.2019.01.221.

Fabbri, A.G. and Chung, C.J., 2019. Landslide susceptibility prediction maps: From blind-testing to uncertainty of class membership: A review of past and present developments. In: Pourghasemi, H.R. and Rossi, M. (Eds.), *Natural Hazards GIS-Based Spatial Modeling Using Data Mining Techniques*. Springer International Publishing, pp. 127–144. https://doi.org/10.1007/978-3-319-73383-8_6.

Gu, X.B., Ma, Y., Wu, Q.H., Ji, X.J. and Bai, H., 2022. The risk assessment of landslide hazards in Shiwangmiao based on intuitionistic fuzzy sets-TOPSIS model. *Natural Hazards*, 111(1), pp. 283–303. https://doi.org/10.1007/s11069-021-05053-5.

Gu, Z. and He, C., 2021. Application of fuzzy decision tree algorithm based on mobile computing in sports fitness member management. *Wireless Communications and Mobile Computing*, 21, pp. 1–10. https://doi.org/10.1155/2021/4632722.

Guzzetti, F., 2000. Landslide fatalities and the evaluation of landslide risk in Italy. *Engineering Geology*, 58(2), pp.89–107. https://doi.org/10.1016/S0013-7952(00)00047-8.

Hewitt, K., 1998. Catastrophic landslides and their effects on the Upper Indus streams, Karakoram Himalaya, northern Pakistan. *Geomorphology*, 26(1–3), pp. 47–80. https://doi.org/10.1016/S0169-555X(98)00051-8.

Hong, H., Pourghasemi, H.R. and Pourtaghi, Z.S., 2016. Landslide susceptibility assessment in Lianhua County (China): A comparison between a random forest data mining technique and bivariate and multivariate statistical models. *Geomorphology*, 259, pp. 105–118. https://doi.org/10.1016/j.geomorph.2016.02.012.

Huang, R., 2012. Mechanisms of large-scale landslides in China. *Bulletin of Engineering Geology and the Environment*, 71(1), pp. 161–170. https://doi.org/10.1007/s10064-011-0403-6.

Kargel, J.S., Leonard, G., Crippen, R.E., Delaney, K.B., Evans, S.G. and Schneider, J., 2010. Satellite monitoring of Pakistan's rockslide-dammed Lake Gojal. *Eos, Transactions American Geophysical Union*, 91(43), pp. 394–395. https://doi.org/10.1029/2010EO430002.

Karim, S., Jalileddin, S. and Ali, M.T., 2011a. Zoning landslide by use of frequency ratio method (case study: Deylaman Region). *Middle-East Journal of Scientific Research*, 9(5), pp. 578–583.

Karim, S., Jalileddin, S. and Ali, M.T., 2011b. Zoning landslide by use of frequency ratio method (case study: Deylaman Region). *Middle-East Journal of Scientific Research*, 9(5), pp. 578–583.

Khan, A., Shitao, Z. and Khan, G., 2022. Comparative analysis and landslide susceptibility mapping of Hunza and Nagar Districts, Pakistan. *Arabian Journal of Geosciences*, 15(21), 1644. https://doi.org/10.1007/s12517-022-10865-1.

Kullback, S. and Leibler, R.A., 1951. On information and sufficiency. *The Annals of Mathematical Statistics*, 22(1), pp. 79–86.

Lee, S. and Talib, J.A., 2005. Probabilistic landslide susceptibility and factor effect analysis. *Environmental Geology*, 47(7), pp. 982–990. https://doi.org/10.1007/s00254-005-1228-z.

Mandal, S. and Mondal, S., 2019. Frequency ratio (FR) model and modified information value (MIV) model in landslide susceptibility assessment and prediction. In: Mandal, S. and Mondal, S. (Eds.), *Statistical Approaches for Landslide Susceptibility Assessment and Prediction*. Springer International Publishing, pp. 77–105. https://doi.org/10.1007/978-3-319-93897-4_3.

Mondal, S. and Mandal, S., 2019. Landslide susceptibility mapping of Darjeeling Himalaya, India using index of entropy (IOE) model. *Applied Geomatics*, 11(2), pp. 129–146. https://doi.org/10.1007/s12518-018-0248-9.

Nohani, M., Moharrami, M., Sharafi, M., Khosravi, K., Pradhan, B., Pham, B.T., Lee, J. and Melesse, A.M., 2019. Landslide susceptibility mapping using different GIS-based bivariate models. *Water*, 11(7), 1402. https://doi.org/10.3390/w11071402.

Panahi, M., Rahmati, O., Rezaie, F., Lee, S., Mohammadi, F. and Conoscenti, C., 2022. Application of the group method of data handling (GMDH) approach for landslide susceptibility zonation using readily available spatial covariates. *CATENA*, 208, 105779. https://doi.org/10.1016/j.catena.2021.105779.

Panchal, S. and Shrivastava, A.K., 2022. Landslide hazard assessment using analytic hierarchy process (AHP): A case study of National Highway 5 in India. *Ain Shams Engineering Journal*, 13(3), p. 101626. https://doi.org/10.1016/j.asej.2021.10.021.

Pandey, V.K., Pourghasemi, H.R. and Sharma, M.C., 2020. Landslide susceptibility mapping using maximum entropy and support vector machine models along the highway corridor, Garhwal Himalaya. *Geocarto International*, 35(2), pp.168–187. https://doi.org/10.1080/10106049.2018.1510038.

Pashkov, B.R. and Shvol'man, V.A., 1979. Rift margins of Tethys in the Pamirs: *Geotectonics*, 13.

Pourghasemi, H.R., 2008. Landslide hazard assessment using fuzzy logic (Case Study: A part of Haraz Watershed) [Ph.D. Thesis]. Tarbiat Modarres University International Campus, Iran.

Pourghasemi, H.R., Jirandeh, A.G., Pradhan, B., Xu, C. and Gokceoglu, C., 2013. Landslide susceptibility mapping using support vector machine and GIS at Golestan Province, Iran. *Journal of Earth System Science*, 122(2), pp. 349–369. https://doi.org/10.1007/s12040-013-0282-2.

Pourghasemi, H.R., Mohammady, M. and Pradhan, B., 2012. Landslide susceptibility mapping using an index of entropy and conditional probability models in GIS: Safarood Basin, Iran. *CATENA*, 97, pp. 71–84. https://doi.org/10.1016/j.catena.2012.05.005.

Pradhan, B., 2013. A comparative study on the predictive ability of the decision tree, support vector machine, and neuro-fuzzy models in landslide susceptibility mapping using GIS. *Computers & Geosciences*, 51, pp. 350–365. https://doi.org/10.1016/j.cageo.2012.08.023.

Qin, S.Q., Jiao, J.J. and Wang, S.J., 2001. The predictable time scale of landslides. *Bulletin of Engineering Geology and the Environment*, 59(4), pp. 307–312. https://doi.org/10.1007/s100640000062.

Rao, C.R., 1985. Weighted distributions arising out of methods of ascertainment: What population does a sample represent? In: Atkinson, A.C. and Fienberg, S.E. (Eds.), *A Celebration of Statistics* (pp. 543–569). Springer. https://doi.org/10.1007/978-1-4613-8560-8_24.

Ronneberger, O., Fischer, P. and Brox, T., 2015. U-Net: Convolutional networks for biomedical image segmentation. In: Navab, N., Hornegger, J., Wells, W.M. and Frangi, A.F. (Eds.), *Medical Image Computing and Computer-Assisted Intervention – MICCAI 2015* (pp. 234–241). Springer International Publishing. https://doi.org/10.1007/978-3-319-24574-4_28.

Sajadi, P., Sang, Y.-F., Gholamnia, M., Bonafoni, S. and Mukherjee, S., 2022. Evaluation of the landslide susceptibility and its spatial difference in the whole Qinghai-Tibetan Plateau region by five learning algorithms. *Geoscience Letters*, 9(1), 9. https://doi.org/10.1186/s40562-022-00218-x.

Searle, M.P. and Tirrul, R., 1991. Structural and thermal evolution of the Karakoram crust. *Journal of the Geological Society*, 148(1), pp. 65–82. https://doi.org/10.1144/gsjgs.148.1.0065.

Shafique, M., van der Meijde, M. and Khan, M.A., 2016. A review of the 2005 Kashmir earthquake-induced landslides, from a remote sensing perspective. *Journal of Asian Earth Sciences*, 118, pp. 68–80. https://doi.org/10.1016/j.jseaes.2016.01.002.

Shan, Y., Chen, S. and Zhong, Q., 2020. Rapid prediction of landslide dam stability using the logistic regression method. *Landslides*, 17(12), pp. 2931–2956. https://doi.org/10.1007/s10346-020-01414-6.

Sun, D., Shi, S., Wen, H., Xu, J., Zhou, X. and Wu, J., 2021. A hybrid optimization method of factor screening predicated on GeoDetector and Random Forest for landslide susceptibility mapping. *Geomorphology*, 379, 107623. https://doi.org/10.1016/j.geomorph.2021.107623.

Suzen, M.L. and Doyuran, V., 2004. Data-driven bivariate landslide susceptibility assessment using geographical information systems: A method and application to Asarsuyu catchment, Turkey. *Engineering Geology*, 71(3), pp. 303–321. https://doi.org/10.1016/S0013-7952(03)00143-1.

Tang, R.X., Yan, E.C., Wen, T., Yin, X.M. and Tang, W., 2021. Comparison of logistic regression, information value, and comprehensive evaluating model for landslide susceptibility mapping. *Sustainability*, 13(7), Article 7. https://doi.org/10.3390/su13073803.

Tien Bui, D., Tuan, T.A., Klempe, H., Pradhan, B. and Revhaug, I., 2016. Spatial prediction models for shallow landslide hazards: A comparative assessment of the efficacy of support vector machines, artificial neural networks, kernel logistic regression, and logistic model tree. *Landslides*, 13(2), pp.361–378. https://doi.org/10.1007/s10346-015-0557-6.

van Westen, C.J., Rengers, N., Terlien, M.T.J. and Soeters, R., 1997. Prediction of the occurrence of slope instability phenomena through GIS-based hazard zonation. *Geologische Rundschau*, 86(2), pp. 404–414. https://doi.org/10.1007/s005310050149.

Verma, R. and Sharma, B.D., 2013. Intuitionistic fuzzy Jensen-Rényi divergence: Applications to multiple-attribute decision making. *Informatica*, 37(4), pp. 276-291.

Wu, Y., Ke, Y., Chen, Z., Liang, S., Zhao, H. and Hong, H., 2020. Application of alternating decision tree with AdaBoost and bagging ensembles for landslide susceptibility mapping. *CATENA, 187*, 104396. https://doi.org/10.1016/j.catena.2019.104396

Yan, F., Zhang, Q., Ye, S. and Ren, B., 2019. A novel hybrid approach for landslide susceptibility mapping integrating analytical hierarchy process and normalized frequency ratio methods with the cloud model. *Geomorphology, 327*, pp. 170–187. https://doi.org/10.1016/j.geomorph.2018.10.024

Youssef, A.M. and Pourghasemi, H.R., 2021. Landslide susceptibility mapping using machine learning algorithms and comparison of their performance at Abha Basin, Asir Region, Saudi Arabia. *Geoscience Frontiers, 12*(2), 639–655. https://doi.org/10.1016/j.gsf.2020.05.010

Zadeh, L.A., 1965. Fuzzy sets. *Information and Control, 8*(3), 338–353. https://doi.org/10.1016/S0019-9958(65)90241-X

Zhang, S., Zhang, L.M., Peng, M., Zhang, L.L., Zhao, H.F. and Chen, H.X., 2012. Assessment of risks of loose landslide deposits formed by the 2008 Wenchuan earthquake. *Natural Hazards and Earth System Sciences, 12*(5), 1381–1392. https://doi.org/10.5194/nhess-12-1381-2012.

Zhang, X., Song, J., Peng, J. and Wu, J., 2019. Landslides-oriented urban disaster resilience assessment—A case study in Shenzhen, China. *Science of The Total Environment, 661*, 95–106. https://doi.org/10.1016/j.scitotenv.2018.12.074

Zhang, Z., Zhou, A., Huang, P., Yang, R. and Ma, C., 2021. Using AHP-VW model to evaluate the landslide susceptibility-A case study of Zigui County, Hubei Province, China. *Arabian Journal of Geosciences, 14*(20), 2095. https://doi.org/10.1007/s12517-021-08476-3

Zou, Y. and Xiao, Z., 2008. Data analysis approaches of soft sets under incomplete information. *Knowledge-Based Systems, 21*(8), 941–945. https://doi.org/10.1016/j.knosys.2008.04.004

ORCID DETAILS OF THE AUTHORS

A. Khan: https://orcid.org/0000-0003-0401-3020